Characterization of subwavelength elastic cylinders with the decomposition of the time-reversal operator: Theory and experiment

Jean-Gabriel Minonzio and Claire Prada
Laboratoire Ondes et Acoustique, Université Denis Diderot, UMR CNRS 7587 ESPCI, 10 rue Vauquelin, 75231 PARIS Cedex 05, France

David Chambers[a)]
Department of Electrical and Computer Engineering, University of California Santa Barbara, Santa Barbara, California

Dominique Clorennec and Mathias Fink
Laboratoire Ondes et Acoustique, Université Denis Diderot, UMR CNRS 7587 ESPCI, 10 rue Vauquelin, 75231 PARIS Cedex 05, France

(Received 9 January 2004; revised 6 September 2004; accepted 9 September 2004)

The decomposition of the time-reversal operator provides information on the scattering medium. It has been shown [Chambers and Gautesen, J. Acoust. Soc. Am. **109**, 2616–2624 (2001)] that a small spherical scatterer is in general associated with four eigenvalues and eigenvectors of the time-reversal operator. In this paper, the 2D problem of scattering by an elastic cylinder, imbedded in water, measured by a linear array of transducers is considered. In this case, the array response matrix has three nonzero singular values. Experimental results are obtained with linear arrays of transducers and for wires of different diameters smaller that the wavelength. It is shown how the singular value distribution and the singular vectors depend on the elastic velocities c_L, c_T, the density ρ of each wire, and on the density ρ_0 and velocity c_0 of the surrounding fluid. These results offer a new perspective towards solution of the inverse problem by determining more than scattering contrast using conventional array processing like that used in medical ultrasonic imaging. © *2005 Acoustical Society of America.* [DOI: 10.1121/1.1811471]

PACS numbers: 43.60.Pt, 43.28.We, 43.20.Fn [DRD] Pages: 789–798

I. INTRODUCTION

The analysis of acoustic scattering is an important tool for object identification. It has applications among nondestructive evaluation, medical imaging, or underwater acoustics. The DORT method is a new approach to scattering analysis that was developed in 1994. It was derived from the theoretical analysis of acoustic time-reversal mirror (TRM) used in the pulse echo mode. DORT is the French acronym for Décomposition de l'Opérateur de Retournement Temporel. It consists of the determination of the invariants of the time-reversal operator (TRO). It was applied to detection and selective focusing through nonhomogeneous multiple targets media.[1,2] It has also been applied to nondestructive evaluation,[3] and characterization of a cylindrical shell through the analysis of the circumferential Lamb modes.[4] While the time-reversal mirror has been shown to be very interesting for spatial and temporal focusing in shallow water,[5–7] the DORT method has also shown high potential for highly resolved detection in a water waveguide.[8–10] This method applies to all type of linear waves and it appears to be interesting for electromagnetic scattering and inverse problem.[11,12]

For all these applications, a good understanding of the invariants of the time-reversal operator is required. Some experimental results obtained in a former study revealed the multiplicity of the invariant of the time-reversal operator for a rigid cylinder immersed in water.[13] In the present paper, we study these invariants for elastic cylinders theoretically and experimentally. In Sec. II, we derive an expression for the array response matrix **K** in two dimensions for the case of a linear array and an elastic cylinder in a fluid medium. The singular value decomposition (SVD) is applied to **K** to determine the number of singular values generated by the cylinder. For the particular case of low frequency (small cylinder), analytic expressions for the singular values and singular vectors are obtained and used to interpret the acoustic scattering mechanism that generates each eigenstate of the time-reversal operator. We use the approach found in recent analyses of time reversal for spheres.[14,15] We will develop the theory for a discrete array at a single frequency ω and then give the final results. In Sec. III, experimental results for thin steel and nylon cylinders are described. It is shown that the analysis of singular values and singular vectors of the transfer matrix **K** offers the possibility to characterize cylinders of subwavelength diameter.

[a)]Correspondence address: Lawrence Livermore National Laboratory, P.O. Box 808, L-154, Livermore, CA 94551.

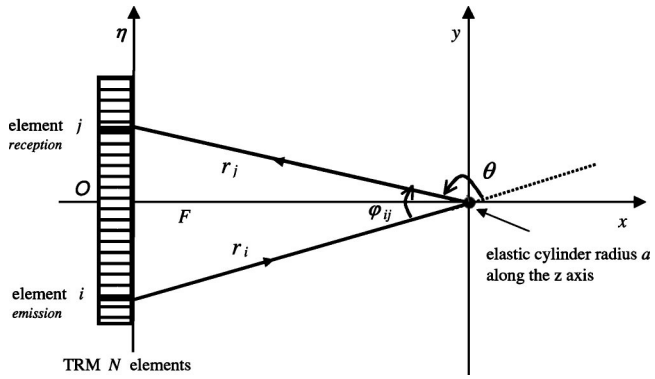

FIG. 1. Geometry of the experiment: F is the distance between the elastic cylinder and the array. The cylinder is perpendicular to the plane insonified by the N-elements array.

II. THEORY

A. Reduced array response matrix for an isotropic scatterer

First of all, an array of N transmit–receive transducers insonifying a static scattering medium is considered as a linear, time-invariant system of N inputs and N outputs. It is characterized at each frequency ω by the array response matrix $\mathbf{K}(\omega)$. The matrix $\mathbf{K}^*(\omega)\mathbf{K}(\omega)$ is called the time-reversal operator,[1] TRO (the notation* means complex conjugate). Its eigenvectors can be interpreted as invariants of the time-reversal process.

As discussed in several papers,[16] if the scattering medium contains a single isotropic scatterer, the array response matrix is easily written as the product of three elements:

(i) a propagation vector of size $N\times 1$, written $\mathbf{H}$, that describes the transmission and the propagation from the N transducers to the scatterer. The coefficient H_i of the vector corresponds to the Fourier transform of the impulse response from transducer number i to the scatterer.
(ii) a scattering coefficient c, which corresponds to the reflectivity of the scatterer.
(iii) a backpropagation vector which is ${}^t\mathbf{H}$ due to the reciprocity principle. The notation ^{t} is used for the transpose operation.

The array response matrix is then

$$\mathbf{K}=\mathbf{H}c\,{}^t\mathbf{H}. \tag{1}$$

We see that in the case of a single isotropic scatterer, things are very simple: the expression above provides directly the singular value decomposition (SVD) of $\mathbf{K}$. In this particular case, there is one nonzero singular value c, and one singular vector $\mathbf{H}$.

We now introduce a reduced array response matrix that will be used in the following analysis. Assuming $k_0F\gg 1$, where F is the distance between the scatterer and the array, and k_0 is the wave number in water (Fig. 1), we can use the far-field form (large argument) of the propagation Green's function in two dimensions in the expression for element number i of the propagation vector

$$H_i(\omega)=\sqrt{\frac{2}{i\pi k_0}}\frac{e^{ik_0r_i}}{\sqrt{r_i}}. \tag{2}$$

For that case, the 2D cylindrical Green's function is the Hankel function. Note that r_i is the distance from the scatterer to the transducer number i. Each element of the array response matrix is then

$$K_{ij}(\omega)=p_0\frac{2}{i\pi k_0}\frac{e^{ik_0r_i}}{\sqrt{r_i}}\frac{e^{ik_0r_j}}{\sqrt{r_j}}c, \tag{3}$$

where p_0 is the amplitude of the pressure emitted by a transducer. We introduce the matrix of the phase terms $\mathbf{T}$. It contains the N phase element $e^{ik_0r_i}$ corresponding to the propagation between the transducer number i and the scatterer, i.e., a diagonal coefficient is $T_{ii}=e^{ik_0r_i}$. $\mathbf{T}$ is unitary and diagonal. It is possible to write the array response matrix as

$$\mathbf{K}(\omega)=p_0\frac{2}{i\pi k_0}\mathbf{T}\mathbf{K}^{\text{reduced}}(\omega)\mathbf{T}. \tag{4}$$

An element of the reduced array response matrix is then written

$$K_{ij}^{\text{reduced}}(\omega)=\frac{c}{\sqrt{r_ir_j}}. \tag{5}$$

In the case of a single isotropic scatterer, this reduced matrix is real and symmetrical. Thus, the singular value decomposition is reduced to diagonalization. We shall see that this reduction is always possible in the far-field approximation and we shall use it for simplicity in the case of anisotropic scatterer.

B. Reduced array response matrix for an elastic cylinder

The pressure field scattered by an elastic cylinder, even for a small cylinder, is not isotropic. In far-field conditions, the field scattered from a plane wave is given, in polar coordinates r and θ, by a sum of partial waves[18,19]

$$P_{\text{sca}}(r,\theta)=p_0\sqrt{\frac{2}{i\pi k_0r}}e^{ik_0r}\sum_{n=0}^{\infty}\epsilon_nR_n\cos(n\theta), \tag{6}$$

where R_n are the scattering coefficients, θ is the angle at the origin between the field point and direction of the incident plane wave, and r is the distance between the scatterer and the field point (Fig. 1). The Neumann coefficients are $\epsilon_0=1$ and $\epsilon_n=2$ for $n\geqslant 1$. As before, we have used the far-field form of the field, replacing the Hankel functions with their asymptotic expressions for large arguments. The scattering coefficients are the coefficients found in Flax *et al.*[18] These are functions of the physical parameters of the cylinders, density ρ_1, radius a, transverse and longitudinal wave speeds (c_T and c_L), and the physicals parameters of the fluid surrounding, velocity c_0 and density ρ_0.

Each term of the sum corresponds to a partial wave, or normal mode. The first term R_0 produces a monopole wave that is circularly symmetric. The second term $2R_1\cos(\theta)$ produces a dipole partial wave, the third term $2R_2\cos(2\theta)$ a quadrupole partial wave, and so on. Thus, the values of the

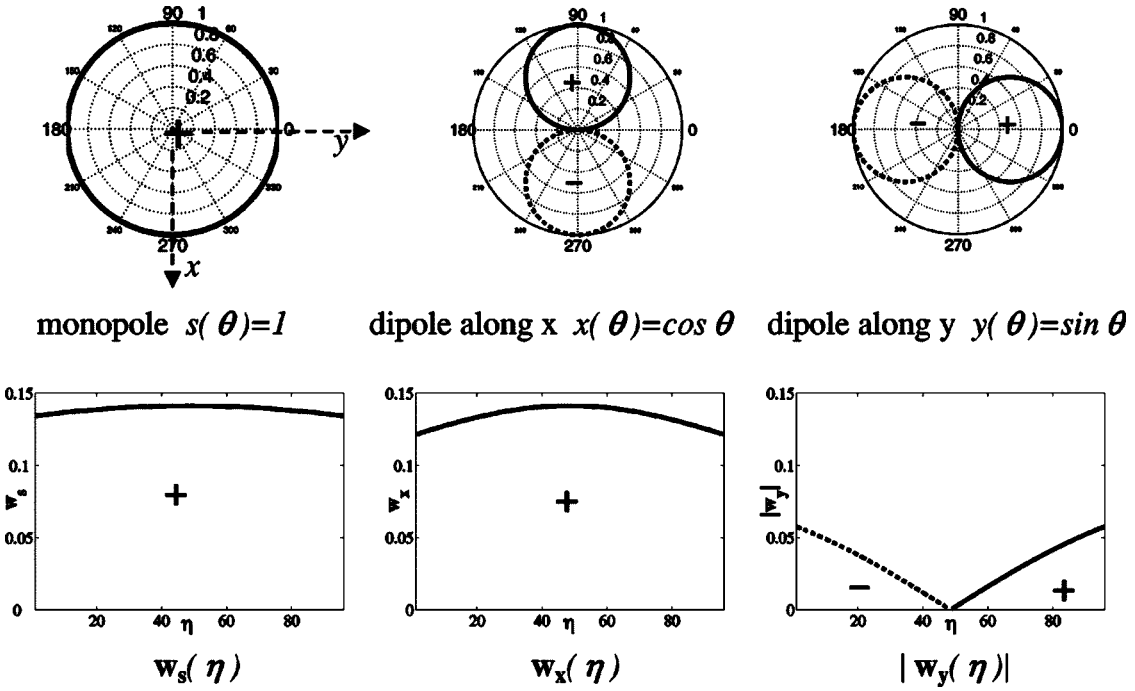

FIG. 2. Normal modes in polar coordinates and their projections onto the array: The normal modes *s*, *x*, and *y* are orthogonal, whereas the projections $\mathbf{w}_s$, $\mathbf{w}_x$, and $\mathbf{w}_y$ are not. The projected modes $\mathbf{w}_s$ and $\mathbf{w}_x$ are symmetric around the *x* axis, whereas $\mathbf{w}_y$ is antisymmetric.

R_n coefficients determine the shape of the scattered field. Let η denote the position along the axis of the array, with η_i the position of transducer number *i*. The position vectors for transducers *i* and *j* are $\mathbf{r}_i=\begin{bmatrix}-F\\ \eta_i\end{bmatrix}$ and $\mathbf{r}_j=\begin{bmatrix}-F\\ \eta_j\end{bmatrix}$, with the angle between them given by $\cos(\varphi_{ij})=(\mathbf{r}_i\cdot\mathbf{r}_j)/r_ir_j=(F^2+\eta_i\eta_j)/r_ir_j$. If the radius *a* of the cylinder is much smaller than the distance to the array ($a\ll F$), the field emitted from transducer *i* is a plane wave at the cylinder, and the scattered field received by transducer *j* will be given by Eq. (6) with $\theta=\pi-\varphi_{ij}$. Using $\cos(n\theta)=(-1)^n\cos(n\varphi_{ij})$, the reduced array response matrix for the case of a single elastic scattering cylinder can be written as

$$K_{ij}^{\text{reduced}}(\omega)=\frac{1}{\sqrt{r_ir_j}}\sum_{n=0}^{\infty}\epsilon_nR_n(-1)^n\cos(n\varphi_{ij}). \tag{7}$$

We notice that the expressions for the reduced array response matrices for isotropic or anisotropic scatterers are similar, in far-field conditions. We introduce the scattering coefficient C_{ij} equal to the sum $\Sigma_{n=0}^{\infty}\epsilon_nR_n(-1)^n\cos(n\varphi_{ij})$, where C_{ij} is an element of the $N\times N$ matrix $\mathbf{C}$. Thus, the general form for an element of the reduced array response matrix is

$$K_{ij}^{\text{reduced}}(\omega)=\frac{C_{ij}}{\sqrt{r_ir_j}}. \tag{8}$$

Note that the matrix $\mathbf{C}$ reduces to a scalar *c* in the case of an isotropic scatterer. It is independent of the positions of the transducers *i* and *j* with respect to the scatterer and $\mathbf{K}^{\text{reduced}}$ is rank 1. For the elastic cylinder, $\mathbf{C}$ is a matrix defined by the infinite sum. The rank of $\mathbf{K}^{\text{reduced}}$ depends on the number of significant R_n. We shall see that if only R_0 and R_1 are significant, $\mathbf{K}^{\text{reduced}}$ is rank 3.

C. Reduced array response matrix for a small elastic cylinder

Though the sum is formally over an infinite number of terms, the coefficients for $n\gg k_0a$ are exponentially small and the sum can be truncated with little error.[15] For the case of a thin cylinder ($k_0a\ll1, k_La\ll1, k_L=\omega/c_L$), the scattering for $n\geqslant2$ can be ignored[18] and the scattered pressure becomes

$$P_{\text{sca}}(r_j,\varphi_{ij})=p_0\sqrt{\frac{2}{i\pi k_0r_j}}e^{ik_0r_j}\left(R_0-2R_1\cos\varphi_{ij}+o\left(2\pi\frac{a}{\lambda}\right)\right). \tag{9}$$

The two first scattering coefficients are[20]

$$R_0=i\frac{\pi k_0^2a^2}{4}\left(\frac{\rho_0c_0^2}{\rho_1(c_L^2-c_T^2)}-1\right)=i\frac{\pi k_0^2a^2}{4}\left(\frac{B_0}{\lambda+\mu}-1\right), \tag{10}$$

$$R_1=-i\frac{\pi k_0^2a^2}{4}\frac{\rho_1-\rho_0}{\rho_1+\rho_0}. \tag{11}$$

In this approximation an element of the reduced scattering matrix becomes (omitting the term $-i[\pi k_0^2a^2/4]$)

$$K_{ij}^{\text{reduced}}(\omega)=\frac{1}{\sqrt{r_ir_j}}\left(\alpha+\beta\frac{F^2+\eta_i\eta_j}{r_ir_j}\right). \tag{12}$$

The constants α and β are[20]

$$\alpha=\left(1-\frac{B_0}{\lambda+\mu}\right),\quad \beta=2\frac{\rho_1-\rho_0}{\rho_1+\rho_0}, \tag{13}$$

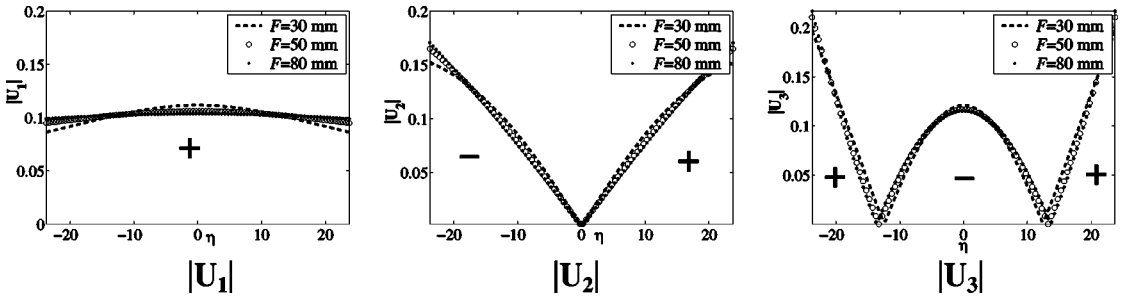

FIG. 3. The three singular vectors $\mathbf{U_1}$, $\mathbf{U_2}$, and $\mathbf{U_3}$ are calculated analytically with the small cylinder approximation along the array (η coordinate). Their modulus are ploted for different distances F between the scatterer and the array: 30 mm (--), 50 mm (○), and 80 mm (*). The variations with the distance are weak.

where λ and μ are the Lamé elastic constants of the cylinder, and B_0 is the bulk modulus (inverse of compressibility) of the fluid. For a 2D-elastic medium, the bulk modulus is $B=\lambda+\mu$ [$B=\lambda+(2/3)\mu$ for a 3D-elastic medium]. The term proportional to α represents scattering by the compressibility contrast. It produces a monopolar radiation pattern that is circularly symmetric. The term proportional to β represents scattering by the density contrast, which produces dipolar radiation pattern (Fig. 2).

D. Analysis of reduced array response matrix for a small elastic cylinder

An element of the matrix can be rewritten as the sum of three separable terms

$$K_{ij}^{\text{reduced}}=\alpha\frac{1}{\sqrt{r_i}}\frac{1}{\sqrt{r_j}}+\beta\frac{F}{r_i^{3/2}}\frac{F}{r_j^{3/2}}+\beta\frac{\eta_i}{r_i^{3/2}}\frac{\eta_j}{r_j^{3/2}}. \tag{14}$$

Let $\mathbf{w_s}$, $\mathbf{w_x}$, and $\mathbf{w_y}$ be the three vectors which correspond to the projection of the normal modes on the TRM (Fig. 2). The elements number i of these vectors, corresponding to the transducer number i, are

$$w_s(\eta_i)=\frac{1}{r_i^{1/2}},\quad w_x(\eta_i)=\frac{F}{r_i^{3/2}},\quad w_y(\eta_i)=\frac{\eta_i}{r_i^{3/2}}. \tag{15}$$

We see that $\mathbf{K}^{\text{reduced}}=\alpha\mathbf{w_s}\,{}^t\mathbf{w_s}+\beta\mathbf{w_x}\,{}^t\mathbf{w_x}+\beta\mathbf{w_y}\,{}^t\mathbf{w_y}$, is the sum of three $N\times N$ matrices of rank 1 which implies that the rank of $\mathbf{K}^{\text{reduced}}$ is 3 as long as α and β are nonzero.

Whatever the emitted signal, the measurement of the scattered field is a linear combination of these three projected vectors. The array response matrix can then be expressed in this new basis and the singular vectors $\mathbf{U_i}$ ($\mathbf{i}=1,2,3$) are linear combinations of the $\mathbf{w_n}$ ($\mathbf{n}$ and $\mathbf{m}$ are used for the indexes $\mathbf{s}$, $\mathbf{x}$, or $\mathbf{y}$), $\mathbf{U_i}=\chi_s\mathbf{w_s}+\chi_x\mathbf{w_x}+\chi_y\mathbf{w_y}$. We denote W_{nm} the scalar product between the vectors $\mathbf{w_n}$ and $\mathbf{w_m}$: $W_{nm}=\langle\mathbf{w_n}|\mathbf{w_m}\rangle=\Sigma_{i=1}^{N}w_n(i)w_m(i)={}^t\mathbf{w_n}\cdot\mathbf{w_m}$. In general, the SVD of $\mathbf{K}$ reduces to solving for the eigenvalues and eigenvectors of a 3×3 matrix, expressed in the new basis of the $\mathbf{w_n}$

$$\begin{bmatrix}\alpha W_{ss} & \alpha W_{sx} & \alpha W_{sy}\\ \beta W_{sx} & \beta W_{xx} & \beta W_{xy}\\ \beta W_{sy} & \beta W_{xy} & \beta W_{yy}\end{bmatrix}\begin{bmatrix}\chi_s\\ \chi_x\\ \chi_y\end{bmatrix}=\lambda\begin{bmatrix}\chi_s\\ \chi_x\\ \chi_y\end{bmatrix}. \tag{16}$$

If the position of the cylinder is symmetrical with respect to the array, the matrix simplifies to

$$\begin{bmatrix}\alpha W_{ss} & \alpha W_{sx} & 0\\ \beta W_{sx} & \beta W_{xx} & 0\\ 0 & 0 & \beta W_{yy}\end{bmatrix}\begin{bmatrix}\chi_s\\ \chi_x\\ \chi_y\end{bmatrix}=\lambda\begin{bmatrix}\chi_s\\ \chi_x\\ \chi_y\end{bmatrix}. \tag{17}$$

Thus, the reduced array response matrix for a thin cylinder may have as many as three distinguishable singular values and singular vectors. If the density contrast β is zero, there is only one singular value. The interpretation of the

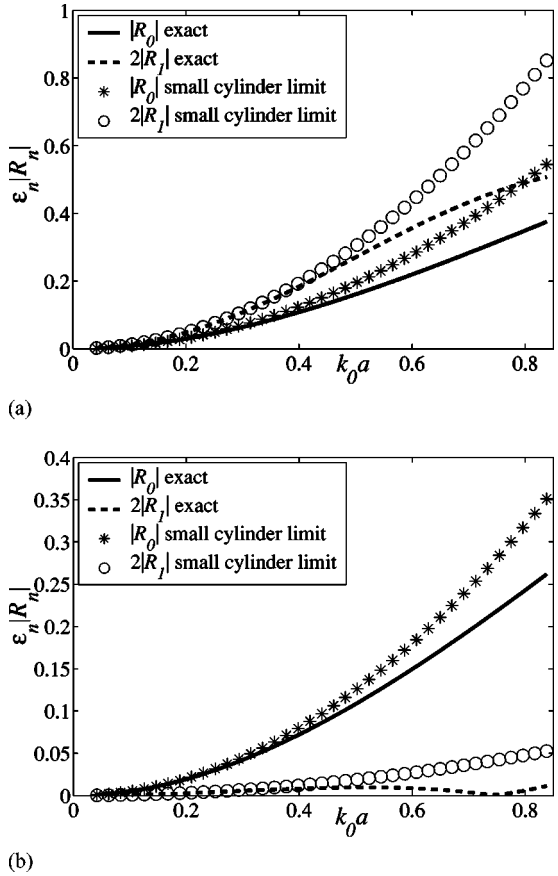

FIG. 4. Coefficients of normal modes $\epsilon_n R_n$ (no dimension) versus $k_0 a$: comparison between the exact value and the approximation for small objects (only the two first coefficients are taken into account). The approximation is valid for $k_0 a$ less than 0.5. In the case of steel (a), the two coefficients R_0 and $2R_1$ are of the same order, whereas, in the case of nylon (b), the second coefficient $2R_1$ is small because of the small density contrast.

TABLE I. Physical parameters of steel and nylon.

	ρ (g·cm^{-3})	c_L (mm·μs^{-1})	c_T (mm·μs^{-1})	α	β	β/α
Steel	7.8	5.75	3	0.99	1.55	1.56
Nylon	1.15	2.5	1.05	0.62	0.14	0.23
Water	1	1.48				

singular values is analogous to that for the sphere studied by Chambers and Gautesen.[14] Three singular values are possible because there are three independent scattering modes: a monopole mode from the compressibility contrast, and two dipole modes from the density contrast. The three singular states of the array response matrix represent three orthogonal combinations of the projected scattering modes.

If the aperture of the array is symmetric around the x axis, the matrix elements W_{sy} and W_{xy} are zero, and simple analytic expressions can be found for the singular values

$$\lambda_{1,3}=\frac{1}{2}(\alpha W_{ss}+\beta W_{xx}) \times\left(1\pm\sqrt{1-4\alpha\beta\frac{W_{ss}W_{xx}-W_{sx}^2}{(\alpha W_{ss}+\beta W_{xx})^2}}\right), \tag{18}$$

$$\lambda_2=\beta W_{yy}. \tag{19}$$

Since $W_{ss}W_{xx}\geqslant W_{sx}^2$ by the Schwarz inequality, the quantity under the radical is always positive[14] and thus, the singular values are real, as required. For our applications $(W_{ss}W_{xx}-W_{sx}^2)/(\alpha W_{ss}+\beta W_{xx})^2\ll 1$, and we can approximate the singular value numbers 1 and 3 as

$$\lambda_1^{\text{app}}\approx\alpha W_{ss}+\beta W_{xx}, \tag{20}$$

$$\lambda_3^{\text{app}}\approx\alpha\beta\frac{W_{ss}W_{xx}-W_{sx}^2}{\alpha W_{ss}+\beta W_{xx}}. \tag{21}$$

Note that the singular values are ordered: $\lambda_1\geqslant\lambda_2\geqslant\lambda_3$. The singular vectors can be written in terms of the $\mathbf{w_n}$

$$\mathbf{U_{1,3}}=\alpha W_{sx}\mathbf{w_s}+(\lambda_{1,3}-\alpha W_{ss})\mathbf{w_x},\quad \mathbf{U_2}=\mathbf{w_y}. \tag{22}$$

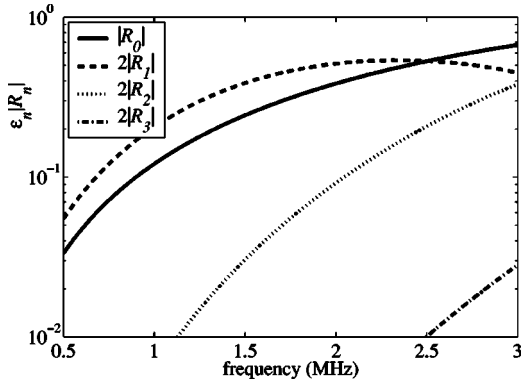

FIG. 5. Coefficients $\epsilon_n R_n$ (no dimension) of the normal modes (logarithm scale) for a steel cylinder of diameter 0.2 mm versus frequency between 0.5 and 3 MHz. The two first coefficients R_0 (monopole) and $2R_1$ (dipole) are predominant in the frequency range. The third one, $2R_2$ (quadrupole), is small and non-negligible for frequencies above 1 MHz. The small object approximation is not valid for that case.

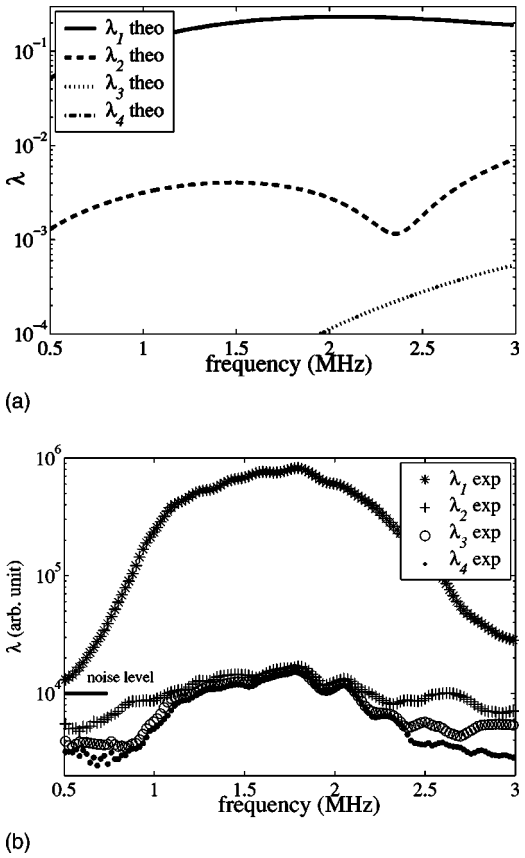

FIG. 6. Singular values λ_n (logarithm scale) for a steel cylinder of diameter 0.2 mm versus frequency: (a) theoretical, the first singular value λ_1 varies slowly in the frequency range. The ratio λ_2/λ_1 lies between 1% and 3%; (b) experimental: the first singular value λ_1 is clearly measured. The second one, λ_2, and the noise are of same order (about 1%).

The two singular vectors $\mathbf{U_1}$ and $\mathbf{U_3}$ are symmetric around the x axis, while $\mathbf{U_2}$ is antisymmetric. Thus, for a symmetric experiment, one singular state represents a dipole oriented parallel to the array, while the other two are orthogonal combinations of the monopole and a dipole oriented normal to the array (Fig. 3).

III. EXPERIMENTAL RESULTS

Experiments have been carried out in a water tank on two materials, steel and nylon, and for different cylinders of

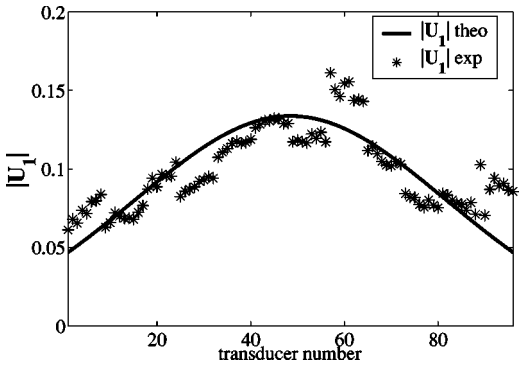

FIG. 7. Modulus of the first singular vector $|\mathbf{U_1}|$ along the array at 1.5 MHz. The difference between theory (continuous line) and experiment (*) is due to the reception level dispersion of the array elements.

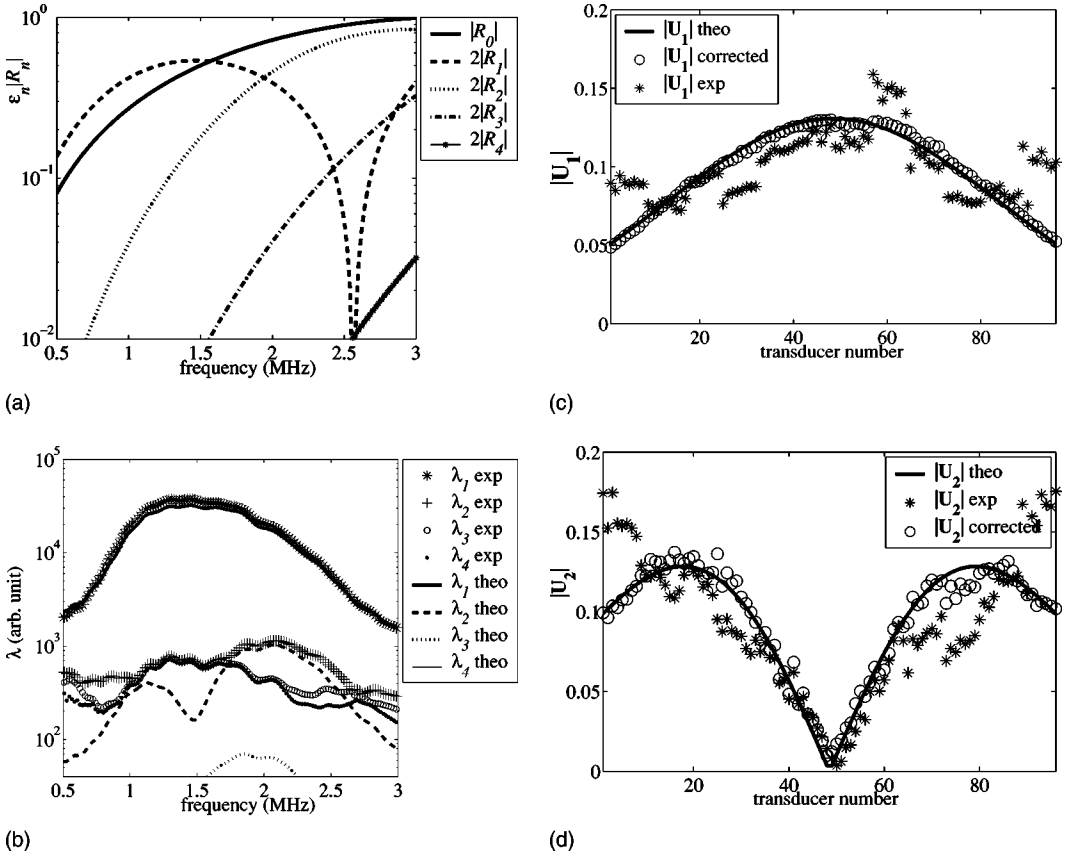

FIG. 8. Results for steel 0.32 mm: (a) coefficients $\varepsilon_n|R_n|$ of normal modes (logarithm scale) versus frequency. The five first coefficients are taken into account in the simulation; (b) simulated (with frequency response) and experimental singular values λ_n (logarithm scale) versus frequency. The experimental second singular value is visible between 1.7 and 2.5 MHz; modulus of the first singular vector $|\mathbf{U_1}|$ (c) and of the second singular vector $|\mathbf{U_2}|$ (d) along the array at 2 MHz: theoretical (continuous line), experimental (*), and reception sensitivity corrected values (○).

diameters between 0.2 and 0.5 mm. The transducer array has 96 elements with central frequency 1.5 MHz, and the array pitch is 0.5 mm. For each experiment, the distance F between the wire and the array is 50 mm. As the cylinder diameters are less than half a wavelength, they have a low scattering power. In order to get a reasonable signal to noise ratio we used the Hadamard–Walsh basis to acquire the array response matrix as explained by Folégot *et al.*[10] This emission basis is very convenient and, in principle, it increases the signal level by a factor of $\sqrt{N}$, N being the number of elements. We also used chirps in order to use the whole bandwidth of the transducers (0.9–2.5 MHz).

The two first coefficients $\varepsilon_n R_n$ for steel and for nylon are shown in Fig. 4. The exact value and the small object approximation of $\epsilon_n R_n$ are compared for $k_0 a$ under 0.8. The expression of approximate coefficients are

$$|R_0|_{\text{app}} = \frac{\pi k_0^2 a^2}{4}\alpha, \quad 2|R_1|_{\text{app}} = \frac{\pi k_0^2 a^2}{2}\beta. \tag{23}$$

The above parabolic approximation [terms are proportional to $(k_0 a)^2$] is valid for $k_0 a$ lower than 0.5. For bigger values of $k_0 a$ the deviation increases. We also remark that in the case of nylon, the β coefficient is small because of the small density contrast (Table I). The frequency band of our system lies between 0.9 and 2.5 MHz, which corresponds to $0.4 < k_0 a < 1.9$. Thus, for the simulations of singular values and vectors, the values of $\epsilon_n R_n$ are calculated with the exact formula given by Flax *et al.*[18] The physical parameters of the cylinders are given in Table I. For comparison to experimental results, the simulation also takes into account the frequency response on transmit and receive and the directivity of each transducer element. The directivity has been measured with a needle probe, and taken into account in the simulations.

A. Steel cylinder, diameter 0.2 mm, a quasi-isotropic scatterer

The first experiment was carried out on the thinnest steel cylinder (diameter 0.2 mm). The coefficients of the normal modes $\varepsilon_n R_n$ for such a cylinder are shown (Fig. 5). The two first coefficients R_0 and $2R_1$ are predominant in the frequency range. The third one, $2R_2$, is small and the others are negligible. We cannot consider that wire as a small object because of the weight of the quadrupole term $2R_2$. In Fig. 6(a), we can see the theoretical singular values calculated for the experimental geometry. The first singular value λ_1 is predominant, the second one λ_2 is very small, and the others are negligible. The ratio λ_2/λ_1 lies between 1% and 3%, in the frequency range [Fig. 6(a)]. In the experimental results the second singular value represents the noise level and we can see in Fig. 6(b) that the noise level is about 3% at the central frequency. So, it is impossible to measure properly the second singular vector.

As the theoretical first singular value varies slowly in the

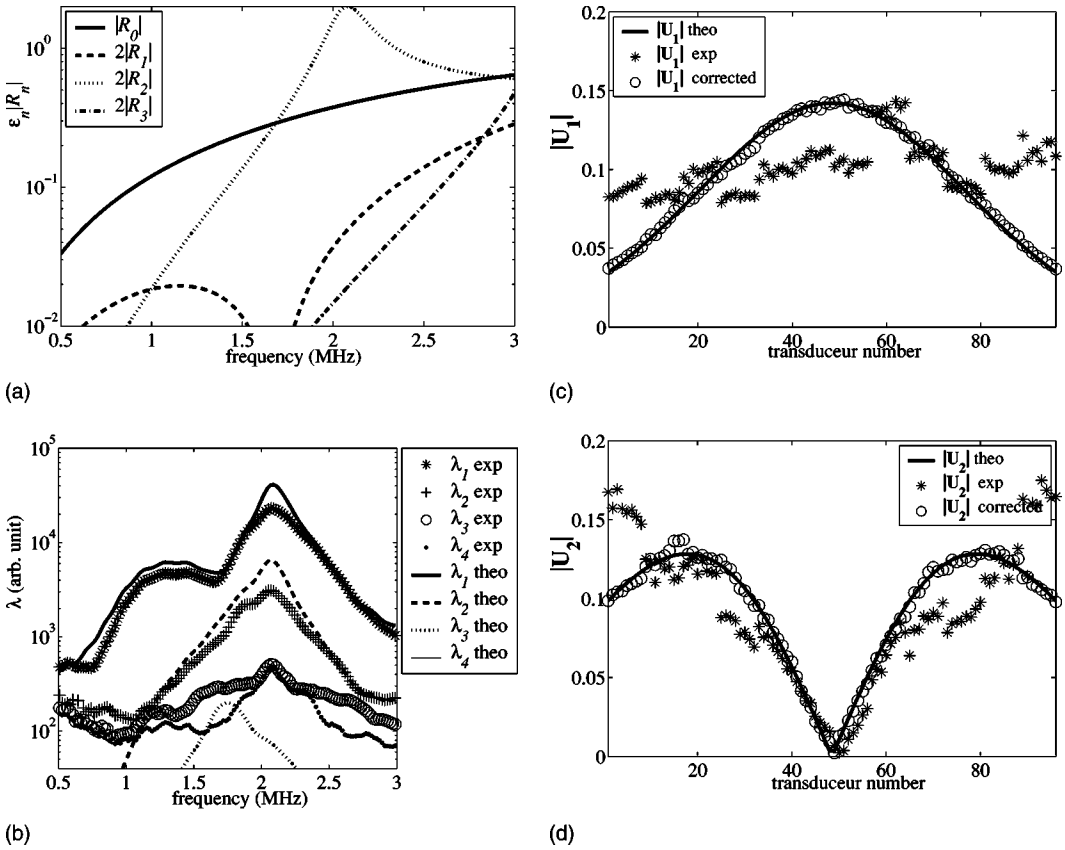

FIG. 9. Results for nylon 0.24 mm: (a) coefficients $\varepsilon_n|R_n|$ of normal modes (logarithm scale) versus frequency; (b) simulated (with frequency response) and experimental singular values λ_n (logarithm scale) versus frequency; modulus of the first singular vector $|\mathbf{U_1}|$ (c) and of the second singular vector $|\mathbf{U_2}|$ (d) along the array at 2.1 MHz.

frequency range, we choose to use this experiment to calibrate our system. The ratio between experimental and theoretical first singular values is used to characterize the frequency response of the system. For the measurement on the other cylinders, the theoretical singular values are multiplied by this ratio to compare them to the experimental ones. We also correct for element sensitivity variations in the array. As we can see for the amplitude of the first singular vector $\mathbf{U_1}$ (Fig. 7), the reception sensitivity varies from one transducer to another. At each frequency, we determine a correction factor from the experimental and theoretical first singular vectors. For the other cylinders, this correction factor was applied frequency by frequency to the array response matrix before computing the SVD.

B. Steel cylinder, diameter 0.32 mm

The second measurement has been carried out on a steel cylinder of diameter 0.32 mm. As we can see in Fig. 8(a), we cannot consider the object as a small scatterer because of the weight of the quadrupole term $2R_2$. The good agreement between the experimental and simulated first singular values λ_1 shows that the frequency response obtained with the smaller steel cylinder is acceptable [Fig. 8(b)]. Figure 8(c) shows the first singular vector $\mathbf{U_1}$. The experimental data (*) show the same reception sensitivity variation as the case of the first steel cylinder (Fig. 7). The corrected data (0) are in good agreement with the simulated singular vector. Thus, the reception correction factor is also acceptable. Figure 8(b) shows that the second experimental singular value λ_2 is generally below the noise level. However, between 1.7 and 2.5, it is clearly above noise, so that we can see the second experimental singular vector $\mathbf{U_2}$ at 2 MHz [Fig. 8(d)].

C. Nylon cylinder, diameter 0.24 mm

The next experiment was carried out on a nylon cylinder of diameter 0.24 mm. We can see in Fig. 9(a) the coefficient of normal modes. The dipole mode coefficient $2|R_1|$ is very small, due to the small density contrast. The quadrupole term $2|R_2|$ has a peak at 2.1 MHz. The peak of the first simulated singular value at 2.1 MHz corresponds to a combination of the monopole, the symmetrical dipole, and quadrupole, the quadrupole contribution being dominant [Fig. 9(b)]. The second experimental singular value λ_2 is clearly above the noise level between 1.2 and 2.5 MHz. So, it is possible to calculate the first two singular vectors $\mathbf{U_1}$ and $\mathbf{U_2}$ [Figs. 9(c) and (d)]. The reception correction is as efficient as for the steel 0.32-mm cylinder.

D. Nylon cylinder, diameter 0.35 mm

The next experiment was carried out on a nylon cylinder of diameter 0.35 mm. We can see in Fig. 10(a) the coefficient of normal modes. The dipole mode coefficient $2|R_1|$ is still very small, due to the small density contrast. The quadrupole term $2|R_2|$ has a peak at 1.52 MHz. The following term $2R_3$

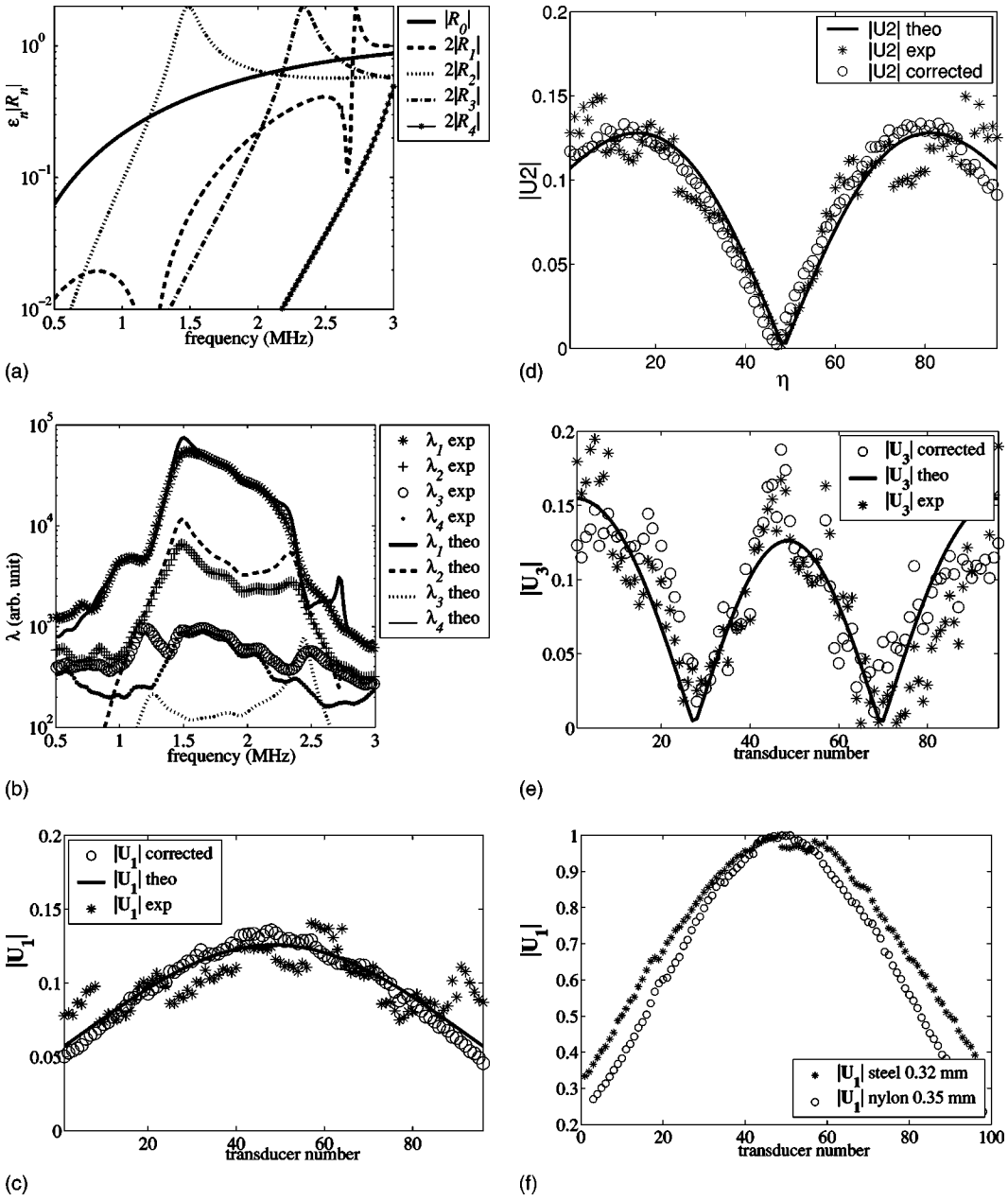

FIG. 10. Results for nylon 0.35 mm: (a) coefficients $\varepsilon_n|R_n|$ of normal modes (logarithm scale) versus frequency; (b) simulated (with frequency response) and experimental singular values λ_n (logarithm scale) versus frequency. The experimental third singular value is above noise around 1 and 2.5 MHz; modulus of the first singular vector $|\mathbf{U_1}|$ (c), of the second singular vector $|\mathbf{U_2}|$ (d) and of the third singular vector $|\mathbf{U_3}|$ (e) along the array at 1.05 MHz; (f) comparison of the modulus of the first singular vector $|\mathbf{U_1}|$ at 1.5 MHz, for a steel wire (0.32 mm:*) and a nylon wire (0.35 mm: ○). Curves are normalized; maxima of the vectors are equal to 1. For a equivalent diameter, the shape difference is due to the coefficients of normal modes. The nylon vector is sharper than the steel one because of the predominant weight of the quadrupole.

is not negligible. The peak of the first simulated singular value at 1.52 MHz corresponds to the quadrupole dominant peak [Fig. 10(b)]. For the two nylon cylinders, that peak corresponds to the same value of k_0a equal to 1.12. But, in that case the peak lies in the middle of the frequency window. The difference between experimental and theoretical peak levels is about 30%, and may be due to a dissipation phenomenon, which is not taken into account in the theory.

We can see in Figs. 10(c) and (d) that there is good agreement between corrected and simulated values for the first two singular vectors $\mathbf{U_1}$ and $\mathbf{U_2}$. The third singular value λ_3 is barely above noise around 1.2 MHz. We observe in Fig. 10(e) that the third singular vector $|\mathbf{U_3}|$ after correction is still noisy, but has a reasonable shape. In Fig. 10(f), we compare the first singular vector for steel (0.32 mm) and nylon (0.35 mm) at 1.5 MHz. The nylon vector is sharper than the steel one because of the predominant weight of the quadrupole. The first singular vector $\mathbf{U_1}$ is a combination of the monopole, the symmetrical dipole, and quadrupole. In the case of nylon at that frequency, the quadrupole contribution is dominant.

E. Nylon cylinder, diameter 0.46 mm

The last experiment was carried out on a nylon cylinder of diameter 0.46 mm. We can see in Fig. 11(a) the coefficient

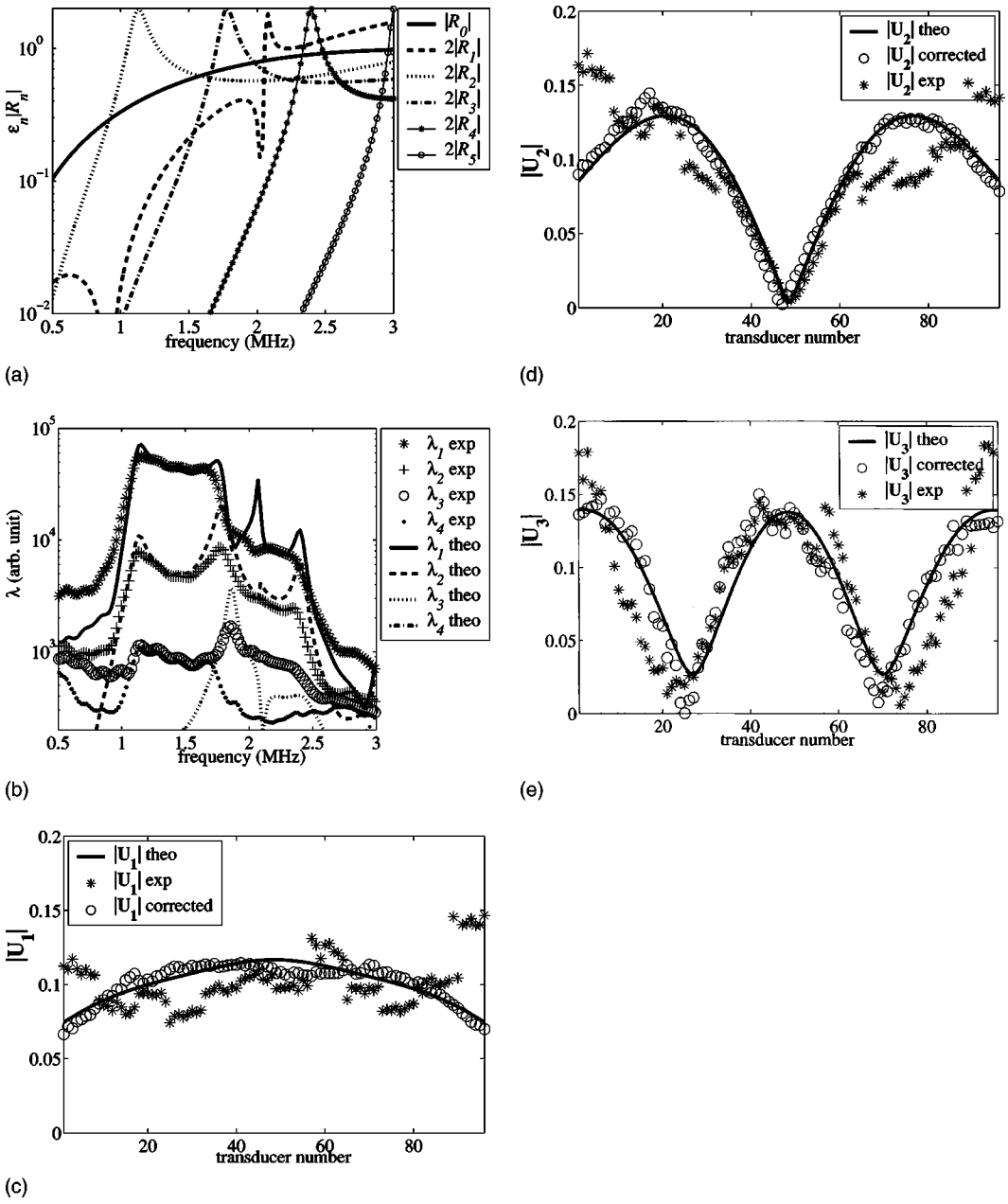

FIG. 11. Results for nylon 0.46 mm: (a) coefficients $\varepsilon_n|R_n|$ of normal modes (logarithm scale) versus frequency; (b) simulated (with frequency response) and experimental singular values λ_n (logarithm scale) versus frequency. The experimental third singular value is above noise around 1.9 MHz; modulus of the first singular vector $|\mathbf{U_1}|$ (c), of the second singular vector $|\mathbf{U_2}|$ (d), of the third singular vector $|\mathbf{U_3}|$ (e) along the array at 1.9 MHz.

of normal modes. The dipole mode coefficient $2|R_1|$ presents a resonance at 2 MHz (π phase jump). The quadrupole term $2|R_2|$ has a peak at 1.14 MHz, corresponding to k_0a equal to 1.12. The following term $2|R_3|$ has a peak at 1.8 MHz. The experimental singular values are in good agreement with simulated ones [Fig. 11(b)], except for the little peaks at 1.17 and 1.74 MHz. Again, the disagreement is probably due to the dissipation phenomenon, which was not taken into account in the simulation.

We can see in Figs. 11(c), (d), and (e) the three singular vectors $\mathbf{U_1}$, $\mathbf{U_2}$, and $\mathbf{U_3}$. There is a good agreement between corrected and simulated values. The third singular value λ_3 is barely above the noise at 1.9 MHz. Figure 12 shows the first three singular values λ_n for the three nylon wires versus k_0a. There is a good agreement between experiment and

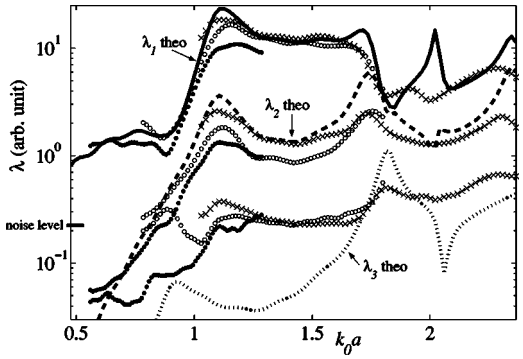

FIG. 12. The first singular values λ_n ($n=1,2,3$) for the three nylon wires are plotted versus k_0a. Experimental values: 0.24-mm diameter wire (·), 0.35-mm diameter wire (°), 0.46-mm diameter wire (×). Theoretical values: first singular value (continuous line), second singular value (dashed line), the third singular values (dotted line). It appears that, if the material of the cylinder is known, its diameter can be deduced from the singular values.

simulation for the three wires. As the noise level is about 1%, we can see that the second experimental singular value is clearly measured for k_0a above 1, and the third one is clearly measured for k_0a above 1.8. Furthermore, it appears that if the material of the cylinder is known, its diameter can be deduced from the singular values.

IV. CONCLUSION

Initially, the DORT method was used assuming a one-to-one correspondence between point-like scatterers and singular vectors of the array response matrix. In Sec. II, we have shown that a subwavelength elastic cylinder is associated with at least three singular vectors and singular values. The singular vectors are a linear combination of normal modes projected onto the array. These combinations are given analytically in the small cylinder limit: the three singular vectors are a combination of the cylindrical mode and two dipolar modes.

In Sec. III, this paper presents the first experimental results showing the multiple singular values for subwavelength scatterers. Five different scatterers were compared at frequencies between 0.9–2.5 MHz: a 0.2- and a 0.32-mm steel cylinder and 0.24-, 0.35-, and 0.46-mm nylon cylinders. Experimental results are in good agreement with theory when several normal modes were taken into account. Different behaviors of nylon and steel are clearly shown. For the steel cylinders, the second eigenvalue was much smaller than the first and contributed little to the scattering. For the nylon cylinders, the second eigenvalue was significant but was generated by a combination of the monopole and quadrupole terms. The dipole term was negligible since the density contrast was small. These results show how the material properties of the cylinder affect the decomposition of the TRO. This opens a new approach to target characterization and the inverse problem based on the analysis of the TRO.

[1] C. Prada and M. Fink, "Eigenmodes of the time reversal operator: a solution to selective focusing in multiple-target media," Wave Motion **20**, 151–163 (1994).

[2] C. Prada, S. Manneville, D. Spoliansky, and M. Fink, "Decomposition of the time reversal operator: Application to detection and selective focusing on two scatterers," J. Acoust. Soc. Am. **99**, 2067–2076 (1996).

[3] E. Kerbrat, C. Prada, D. Cassereau, R. K. Ing, and M. Fink, "Detection and imaging in complex media with the D.O.R.T. method," IEEE Ultrasonic Symposium Proceedings, 779–783 (2000).

[4] C. Prada and M. Fink, "Separation of interfering acoustic scattered signals using the invariant of the time-reversal operator. Application to Lamb waves characterization," J. Acoust. Soc. Am. **104**(2), 801–807 (1998).

[5] D. R. Jackson and D. R. Dowling, "Phase conjugation in underwater acoustics," J. Acoust. Soc. Am. **89**(1), 171–181 (1991).

[6] W. A. Kuperman, W. S. Hodgkiss, H. C. Song, T. Akal, C. Ferla, and D. R. Jackson, "Phase conjugation in the ocean: Experimental demonstration of an acoustic time-reversal mirror," J. Acoust. Soc. Am. **103**(1), 25–40 (1998).

[7] S. R. Khosla and D. R. Dowling, "Time-reversing array retrofocusing in noisy environments," J. Acoust. Soc. Am. **109**(2), 538–546 (2001).

[8] N. Mordant, C. Prada, and M. Fink, "Highly resolved detection and selective focusing in a waveguide using the D.O.R.T. method," J. Acoust. Soc. Am. **105**, 2634–2642 (1999).

[9] T. Yokoyama, T. Kikuchi, T. Tsuchiya, and A. Hasegawa, "Detection and selective focusing on scatterers using decomposition of time reversal operator method in Pekeris waveguide model," Jpn. J. Appl. Phys. **40**, 3822–3828 (2001).

[10] T. Folégot, C. Prada, and M. Fink, "Resolution enhancement and separation of reverberation from target echo with the time reversal operator decomposition," J. Acoust. Soc. Am. **113**, 3155–5160 (2003).

[11] H. Tortel, G. Micolau, and M. Saillard, "Decomposition of the time reversal operator for electromagnetic scattering," J. Electromagn. Waves Appl. **13**, 687–719 (1999).

[12] G. Micolau, M. Saillard, and P. Borderies, "DORT as applied to ultrawideband signals for detection of buried objects," IEEE Trans. Geosci. Remote Sens. **41**(8), 1813–1820 (2003).

[13] S. Komilikis, C. Prada, and M. Fink, "Characterization of extended objects with the D.O.R.T. method," IEEE Ultrasonic Symposium Proceedings, 1401–1404 (1996).

[14] D. H. Chambers and A. K. Gautesen, "Time reversal for a single spherical scatterer," J. Acoust. Soc. Am. **109**, 2616–2624 (2001).

[15] D. H. Chambers, "Analysis of the time-reversal operator for scatterers of finite size," J. Acoust. Soc. Am. **112**, 411–419 (2002).

[16] C. Prada, "Detection and imaging in complex media with the D.O.R.T. method," in *Imaging of Complex Media with Acoustic and Seismic Waves*, Topics Appl. Phys. Vol. 84 (Springer, Berlin, 2002), pp. 107–133.

[17] W. F. Walker, "C- and D-weighted ultrasonic imaging using the translating aperture algorithm," IEEE Trans. Ultrason. Ferroelectr. Freq. Control **48**(2), 452–461 (2001).

[18] L. Flax, G. Gaunard, and H. Überall, "Theory of resonance scattering," *Physical Acoustics*, edited by W. Mason and R. Thurston (Academic Press, New York, 1976), Vol. XV, pp. 191–294.

[19] A. Derem, "N. Gespa La diffusion acoustique par des cibles géométriques de forme simple Théories et expériences," Cedocar Chap. 9, 196–200 (1987).

[20] R. Doolittle and H. Überall, "Sound scattering by elastic cylindrical shells," J. Acoust. Soc. Am. **39**, 272–275 (1965).